Semiclassical theory of sub-Doppler forces in an asymmetric magneto-optical trap with unequal laser detunings

Heung-Ryoul Noh[1] and Wonho Jhe[2,*]

[1]*Department of Physics and Institute of Opto-Electronic Science and Technology, Chonnam National University, Gwangju 500-757, Korea*

[2]*Department of Physics and Astronomy, Seoul National University, Seoul 151-747, Korea*

(Received 20 January 2007; published 17 May 2007)

We present a semiclassical theory of the sub-Doppler forces in an asymmetric magneto-optical trap where the trap-laser frequencies are unequal to one another. To solve the optical Bloch equations, which contain explicit time dependence, unlike in the symmetric case of equal laser detunings, we have developed a convenient and efficient method to calculate the atomic forces at various oscillating frequencies for each atomic density matrix element. In particular, the theory provides a qualitative understanding of the array of sub-Doppler traps (SDTs) recently observed in such an asymmetric trap. We find that the distances between SDTs are proportional to the relative detuning differences, in good agreement with experimental results. The theory presented here can be applied to a dynamic system with multiple laser frequencies involved; the number of coupled equations to solve is much reduced and the resulting numerical calculation can be performed rather simply and efficiently.

DOI: 10.1103/PhysRevA.75.053411 PACS number(s): 32.80.Pj, 39.25.+k, 03.75.Be, 42.50.Vk

I. INTRODUCTION

Since laser cooling of neutral atoms was first proposed [1], there have been many advances in manipulating neutral atoms by laser light [2]. Among the various techniques, the magneto-optical trap (MOT) is known to be one of the simplest ways to obtain cold atoms [3]. Although the MOT has been widely used as a well-established precooled atom source, it still provides vast unexplored research subjects, such as nonlinear dynamics [4], instability-induced atomic pulsation [5], or the spontaneous symmetry breaking of an atomic population [6].

In particular, one of the interesting characteristics of the MOT itself is the intrinsic property of the sub-Doppler temperature therein [7–9]. It is well known that there exist two kinds of forces in the MOT: a Doppler cooling force as well as a sub-Doppler one [10]. The Doppler force originates from the difference of the scattering rates of a moving atom from the counterpropagating laser beams and exists within a broad range of velocity and position space. On the contrary, the sub-Doppler force results from the coherences between the magnetic sublevels of the ground state and exists in the vicinity of the origin of the phase space. The latter plays an important role in obtaining low atomic temperatures down to approximately 10 μK, or the corresponding high density of an atomic cloud [11].

Recently, we have investigated the trap parameters when the detunings of the trap-laser beams propagating along the transverse axes are different from those on the horizontal (z) axis [12]. We observed experimentally that, when the relative laser detunings are different, the sub-Doppler force gradually disappears, resulting in an abruptly decreased damping coefficient, approaching the value expected in simple Doppler theory. Also we found that, as the intensity of the transverse laser beams increases, new sub-Doppler traps appear at symmetric positions with respect to the MOT center, and their displacements from the center are proportional to the detuning differences. In this paper, we present a semiclassical theory of the sub-Doppler forces in a two-dimensional MOT, where two differing laser frequencies are involved. The theory can be easily extended to a general atomic dynamics system containing multiple laser frequencies.

Calculation of the atomic dynamics in the presence of bichromatic or multichromatic laser beams has been performed in several studies [13–16]. In that research, the density matrix elements were expanded by Fourier series in terms of the frequency differences. Instead of direct calculation of all the Fourier components, however, we have formulated an alternative method to find the nonvanishing Fourier components as described in Sec. III. Since we retain only the nonvanishing elements, the number of coupled equations to solve is greatly reduced, and accordingly the numerical calculation can be simpler and more efficient than the methods described in Refs. [13–16]. Moreover, the theoretical method that we have developed can be extended to arbitrary accuracy by increasing the number of iterations.

The paper is organized as follows. In the next section, we present the general theoretical frame to calculate the atomic forces. Then a detailed explanation of how to obtain the oscillation frequencies of all the density matrix elements follows. In Sec. IV, we present the calculated results in various conditions, and summarize the calculated results in the last section.

II. METHOD OF CALCULATION

Here we present the calculation of the semiclassical sub-Doppler forces in two dimensions. In order to calculate the force, one has to solve the following optical Bloch equation [17]:

*Electronic address: whjhe@snu.ac.kr

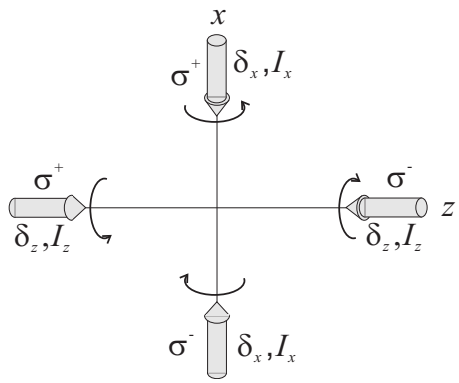

FIG. 1. Two-dimensional laser configuration. The circularly polarized laser beams on the z and x axes have different frequencies. A constant magnetic field B is applied along z axis.

$$i\hbar\frac{\partial\rho}{\partial t} = [H_0 + V, \rho] + i\hbar\left(\frac{\partial\rho}{\partial t}\right)_{sp}, \tag{1}$$

where ρ is the density matrix operator, and the atomic Hamiltonian H_0 is given by

$$H_0 = \hbar\sum_{m_e=-F_e}^{F_e}(\omega_0 + \omega_B m_e g_e)|e_{m_e}\rangle\langle e_{m_e}| + \hbar\sum_{m_g=-F_g}^{F_g}\omega_B m_g g_g \times |g_{m_g}\rangle\langle g_{m_g}|. \tag{2}$$

Here ω_0 is the atomic resonance frequency, g_e (g_g), m_e (m_g), and F_e (F_g) are the Landé g factor, the quantum number of the magnetic sublevels, and the angular momentum of the excited (ground) state, respectively. We also included the Zeeman shift $\omega_B = \mu_B B/\hbar$, where B is the magnitude of the magnetic field directed along the z direction.

The laser scheme under consideration is shown in Fig. 1. We assume that an atom moves along the z direction with a velocity of v and, in the atomic rest frame, experiences an electric field given by

$$\vec{E}(x,z) = \frac{E_z}{2}\hat{\epsilon}_+ e^{ik_z z - i(\omega_z - k_z v)t} + \frac{E_z}{2}\hat{\epsilon}_- e^{-ik_z z - i(\omega_z + k_z v)t} + \frac{E_x}{2}\hat{\epsilon}_-^x e^{ik_x x - i\omega_x t} + \frac{E_x}{2}\hat{\epsilon}_+^x e^{-ik_x x - i\omega_x t} + \text{c.c.}, \tag{3}$$

where ω_i, k_i, and E_i are the angular frequency, the wave vector, and the amplitude of the electric field on the i axis ($i = z, x$), respectively, and $\epsilon_\pm$ ($\epsilon_\pm^x$) represents the polarization of $\sigma^\pm$ photons propagating in the $\pm z$ ($\mp x$) directions. We define the detuning difference as $\delta = \delta_x - \delta_z$, where $\delta_i = \omega_i - \omega_0$.

Since the polarizations of the laser photons on the x axis are decomposed as

$$\hat{\epsilon}_\pm^x = \mp\frac{1}{\sqrt{2}}(\hat{y} \pm i\hat{z}),$$

where we take z as the quantization axis, the interaction Hamiltonian V is given by

$$V = \sum_{m=-F_g}^{F_g}\sum_{q=0,\pm1}\kappa_q\langle F_e, m+q|1,q;F_g,m\rangle \times |e_{m+q}\rangle\langle g_m| + \text{H.c.}, \tag{4}$$

where

$$\kappa_{\pm1} = \frac{1}{2}\hbar\Omega_z e^{\pm ik_z z}e^{-i(\omega_z \mp k_z v)t} - \frac{1}{2}\hbar\Omega_x \sin k_x x e^{-i\omega_x t},$$

$$\kappa_0 = -\frac{i}{\sqrt{2}}\Omega_x \cos k_x x e^{-i\omega_x t}, \tag{5}$$

with the Rabi frequencies $\Omega_i = -d_{eg}E_i/\hbar$ for $i = z, x$. Here d_{eg} is the matrix element $\langle e_{F_e}|d|g_{F_g}\rangle$ of the dipole moment operator d. The last term in Eq. (1), representing the spontaneous emissions, satisfies the relations

$$\langle e_{m_e}|\left(\frac{\partial\rho}{\partial t}\right)_{sp}|e_{m'_e}\rangle = -\Gamma\langle e_{m_e}|\rho|e_{m'_e}\rangle,$$

$$\langle e_{m_e}|\left(\frac{\partial\rho}{\partial t}\right)_{sp}|g_{m_g}\rangle = -\frac{\Gamma}{2}\langle e_{m_e}|\rho|g_{m_g}\rangle,$$

$$\langle g_{m_g}|\left(\frac{\partial\rho}{\partial t}\right)_{sp}|e_{m_e}\rangle = -\frac{\Gamma}{2}\langle g_{m_g}|\rho|e_{m_e}\rangle,$$

$$\langle g_{m_g}|\left(\frac{\partial\rho}{\partial t}\right)_{sp}|g_{m'_g}\rangle = \Gamma\sum_{q=-1}^{1}\langle F_e, m_g+q|1,q;F_g,m_g\rangle \times \langle F_e, m'_g+q|1,q;F_g,m'_g\rangle\langle e_{m_g+q}|\rho|e_{m'_e+q}\rangle. \tag{6}$$

Finally, the force experienced by an atom at $z = 0$ is given by

$$F = -\left\langle\frac{dV}{dz}\right\rangle = \frac{i}{2}\hbar k_z\Omega_z\sum_{m_g=-F_g}^{F_g}\langle F_e, m_g+1|1,1;F_g,m_g\rangle \times \langle e_{m_g+1}|\rho|g_{m_g}\rangle e^{i(\omega_z - k_z v)t} - \frac{i}{2}\hbar k_z\Omega_z\sum_{m_g=-F_g}^{F_g}\langle F_e, m_g-1|1,-1;F_g,m_g\rangle \times \langle e_{m_g-1}|\rho|g_{m_g}\rangle e^{i(\omega_z + k_z v)t} + \text{c.c.} \tag{7}$$

When we solve Eq. (1), unlike for the case of a single oscillation frequency, it is not possible to obtain equations that do not contain explicit time dependence by a suitable transformation, since there exist two oscillation frequencies. Therefore we have to make an approximation and truncate the equations after a finite number of iterations.

Now let us solve Eq. (1), which can be written as

$$\dot{\rho} = Q^{(1)}, \tag{8}$$

where

$$Q^{(1)} = -\frac{i}{\hbar}[H_0 + V, \rho] + (\dot{\rho})_{sp}. \tag{9}$$

Here $Q^{(1)}$ is a diagonal matrix whose dimension is $F_N \times F_N$, where $F_N = (2F_e+1)+(2F_g+1)$, and the order of the eigen-

states is $|e_{-F_e}\rangle,\ldots,|g_{F_g}\rangle$. Then we transform Eq. (8) to a frame rotating with an angular frequency ω_z, i.e., where the i,j component of ρ is given by $\rho_{ij}=e^{ic_{ij}t}\sigma_{ij}$ and σ_{ij} is the slowly varying density matrix element. $c_{ij}=-\omega_z$ (ω_z) when the states i and j belong, respectively, to the excited and ground (ground and excited) states, whereas $c_{ij}=0$ when i and j belong to the same excited or ground state.

Then Eq. (8) becomes

$$\dot{\sigma}_{ij}=Q_{ij}^{(2)}, \tag{10}$$

where

$$Q_{ij}^{(2)}=e^{-ic_{ij}t}Q_{ij}^{(1)}-ic_{ij}\sigma_{ij}. \tag{11}$$

Since there exist several oscillation frequencies such as $\omega_z\pm kv$ and ω_x, we cannot eliminate the explicit time dependence in Eq. (11). Therefore we expand σ_{ij} in terms of the various oscillation frequencies as follows:

$$\sigma_{ij}=\sum_{k=1}^{b^{(ij)}}A_k^{(ij)}e^{i\zeta_k^{(ij)}t}, \tag{12}$$

where $A_k^{(ij)}$ and $\zeta_k^{(ij)}$ are the kth element of the amplitude vector $A^{(ij)}$ and the oscillation frequency vector $\zeta^{(ij)}$ for given indices (i,j), respectively, and $b^{(ij)}$ is a scalar denoting the number of elements of the vector $\zeta^{(ij)}$.

We now insert Eq. (12) into Eqs. (10) and (11), and define the following function:

$$Q_{ij}=\dot{\sigma}_{ij}-Q_{ij}^{(2)}=\sum_{k=1}^{b^{(ij)}}i\zeta_k^{(ij)}A_k^{(ij)}e^{i\zeta_k^{(ij)}t}-Q_{ij}^{(2)}, \tag{13}$$

where $Q_{ij}^{(2)}$ is expressed in terms of $A_k^{(ij)}$ and $\zeta_k^{(ij)}$. Note that Eq. (13) vanishes identically when $b^{(ij)}$ is an infinite number. In a real situation, however, we have to use a finite number of $b^{(ij)}$. In order to obtain various values of $\zeta_k^{(ij)}$, we have considered interactions that are connected by not more than N photons. If N is an odd (even) number, we can obtain $Q_{ij}=0$ for i and j belonging to different (same) energy states. For example, when we consider the interactions connected by five photons, Q_{eg} and Q_{ge} vanish just as in the case of an infinite number of $b^{(ij)}$, where e (g) denotes the state $|e_{m_e}\rangle$ ($|g_{m_g}\rangle$). However, Q_{ee} and Q_{gg} do not vanish, which implies the existence of some errors in σ_{ee} and σ_{gg}. The final task is then to calculate all the $A_k^{(ij)}$ values by equating the terms with equal oscillation frequencies in Eq. (13).

In the calculation, we have to include the $b^{(ii)}$ equations associated with the normalization conditions (note that $b^{(ii)}$ are the same for all i), as given by

$$\sum_{i=1}^{F_N}A_k^{(ii)}=\begin{cases}1, & k=1,\\ 0, & k=2,\ldots,b^{(ii)}.\end{cases} \tag{14}$$

As will be explained in the next section, one element of $\zeta^{(ii)}$ is 0, which implies the nonoscillation case, and all the other elements are composed of pairs of $\pm c$, where c is a function of δ and k_zv. Then we may define the first element as 0; thus the first element of $A^{(ii)}$ is real, and the other elements are complex. Instead of including the normalization conditions, the same number of equations in Eq. (13) should be ruled out. Since only the nonvanishing elements are included in Eq. (12), the number of coupled equations [Eqs. (13) and (14)] can be significantly reduced compared to the cases in Refs. [13–16]. Therefore, once the oscillation frequencies are obtained as shown in the method of the next section, the calculation can be straightforward. We also note that the off-diagonal elements satisfy $A_k^{(ij)*}=A_k^{(ji)}$.

After we obtain all the values of $A_k^{(ij)}$, we can calculate the density matrix elements as

$$\rho_{ij}=e^{ic_{ij}t}\sum_{k=1}^{b^{(ij)}}A_k^{(ij)}e^{i\zeta_k^{(ij)}t}. \tag{15}$$

Inserting Eq. (15) into Eq. (7), the force then becomes

$$F=-\hbar k_z\Omega_z\sum_{m=-F_g}^{F_g}\langle F_e,m+1|1,1;F_g,m\rangle\times\mathrm{Im}\,A_1^{(e_{m+1},g_m)}+\hbar k_z\Omega_z\sum_{m=-F_g}^{F_g}\langle F_e,m-1|1,1;F_g,m\rangle\times\mathrm{Im}\,A_1^{(e_{m-1},g_m)}, \tag{16}$$

where we have assumed that the first element of $\zeta^{(e_{m\pm1},g_m)}$ is $\pm k_zv$. Since the force in Eq. (16) is obtained after averaging over the time, none of the other components of $A^{(e_{m\pm1},g_m)}$ except the first term contribute to the force.

III. CALCULATION OF THE OSCILLATION FREQUENCIES

In this section, we calculate the various oscillation frequencies $\zeta_k^{(ij)}$ for all of the matrix elements. Let us first define the number of interactions N, which is assumed to be an odd number. The case for even N will be treated later on. Here we calculate the oscillation frequencies of the density matrix element $\langle e_m|\sigma|g_{m+\Delta m}\rangle$ as shown in Fig. 2(a). The procedure of calculations can be summarized as follows. We first obtain all the possible routes connecting the states $|e_m\rangle$ and $|g_{m+\Delta m}\rangle$ within a number of photons not greater than N. Then we calculate the oscillation frequencies by the method described below.

The transition schemes are shown in Fig. 2(b), where the oscillation frequencies with respect to ω_z are (k_zv,δ), $(-k_zv,\delta)$, and δ for σ^-, σ^+, and π transitions, respectively. In the calculation of the oscillation frequencies, we have used the fact that the absorption or emission of each polarized photon contributes to the resulting frequencies according to the rules described in Table I. For instance, let us consider the route shown in Fig. 2(c). In this route, an atom emits a σ^- photon, absorbs a π photon, emits a σ^- photon, absorbs a σ^+ photon, and finally emits a σ^- photon. In this case, the characteristic frequencies are calculated to be

$$(-k_zv,-\delta)+(\delta)+(-k_zv,-\delta)+(-k_zv,\delta)+(-k_zv,-\delta). \tag{17}$$

Since each element in parentheses contributes equally, there exist 2^4 results, including the duplicated ones, and so we

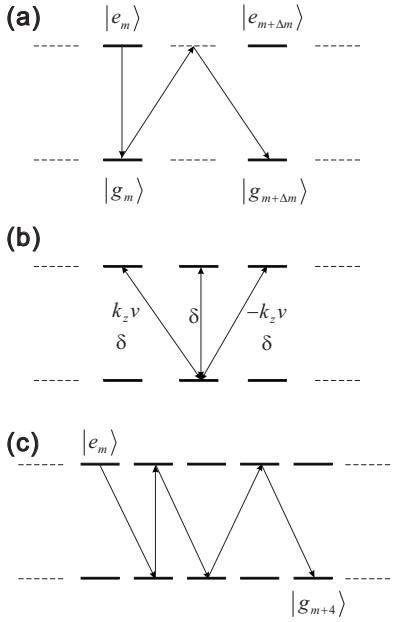

FIG. 2. (a) Scheme of the calculation of the oscillation frequencies of the density matrix elements $\langle e_m|\sigma|g_{m+\Delta m}\rangle$. (b) The oscillation frequencies relevant to each transition. (c) Typical route from $|e_m\rangle$ to $|g_{m+4}\rangle$.

finally obtain eight different frequencies given by $-4k_z v+\delta$, $-3k_z v+2\delta$, $-3k_z v$, $-2k_z v\pm\delta$, $-k_z v-2\delta$, $-k_z v$, and $-\delta$.

We now discuss a systematic method to obtain all the possible routes from the state $|e_m\rangle$ to the state $|g_{m+\Delta m}\rangle$, which can be accomplished by considering the change of the magnetic quantum number for the emission as well as absorption of $\sigma^{\pm}$ or π polarized photons. This can be formulated as

$$\sum_{j=1}^{N}(-1)^j k_j = \Delta m, \tag{18}$$

where the sign -1 $(+1)$ for odd (even) j stands for the emission (absorption) of photons. The alternating behavior of the sign implies the fact that emission and absorption processes occur in a similar alternating fashion. In Eq. (18), the integer k_j represents the polarization of the jth photon, which is ± 1 for $\sigma^{\pm}$ and 0 for a π photon. Therefore, once we obtain the integers $(k_1,k_2,\ldots,k_N)$ satisfying Eq. (18), we can find all the different routes between the two states under consideration. Since there exist many sets of integers $(k_1,k_2,\ldots,k_N)$ corresponding to different routes between the states, we may create a matrix T whose row elements are composed of the integers $(k_1,k_2,\ldots,k_N)$. In other words, T_{ij} is the jth element of the ith set of $(k_1,k_2,\ldots,k_N)$.

TABLE I. The contribution to the resulting frequencies by absorption or emission of the polarized photons.

	σ^+	σ^-	π
Absorption	$-k_z v,\delta$	$k_z v,\delta$	δ
Emission	$k_z v,-\delta$	$-k_z v,-\delta$	$-\delta$

For example, for $\Delta m=4$, the matrix T can be written as

$$T=\begin{pmatrix} -1 & 0 & -1 & 1 & -1 \\ -1 & 1 & -1 & 0 & -1 \\ -1 & 1 & -1 & 1 & 0 \\ -1 & 1 & 0 & 1 & -1 \\ 0 & 1 & -1 & 1 & -1 \end{pmatrix}. \tag{19}$$

Each row of the matrix T in Eq. (19) represents a different route from $|e_m\rangle$ to $|g_{m+\Delta m}\rangle$. For instance, the first row $(-1,0,-1,1,-1)$ represents the route as shown in Fig. 2(c), which was mentioned above.

With the transition schemes shown in Fig. 2(b), in order to find the oscillation frequencies, we define the row matrices $a^{(ij)}$ for given i and j, as follows:

$$a^{(ij)}=\begin{cases}\{k_z v,\delta\}, & T_{ij}=-1,\\ \{\delta\}, & T_{ij}=0,\\ \{-k_z v,\delta\}, & T_{ij}=+1,\end{cases} \tag{20}$$

where T_{ij} is the ijth component of the matrix T. For example, for $T_{ij}=-1$, $a_1^{(ij)}=kv$ and $a_2^{(ij)}=\delta$. Here the indices i and j run from 1 to the number of rows of T and N, respectively. To obtain the oscillation frequencies for a given Δm, we merely have to calculate the following equation for all the possible different sets of $l_1,l_2,\ldots,l_N$, and i:

$$\sum_{j=1}^{N}(-1)^j a_{l_j}^{(ij)} = -a_{l_1}^{(i1)}+a_{l_2}^{(i2)}-+\cdots+(-1)^N a_{l_N}^{(iN)}, \tag{21}$$

where $l_j=1,2$ $(j=1,2,\ldots,N)$ and the row number of the matrix T is $i=1,2,\ldots$. Therefore the number of sets including the null results is $2^N\times$ the number of i. Note that the explicit expression of Eq. (21) for the first row of the matrix T with $\Delta m=4$, for example, is given by Eq. (17). If we perform similar calculations as in Eq. (17) for all other rows of the matrix T, i.e., Eq. (21), while excluding the meaningless terms, we can obtain the elements of the vector $\zeta^{(e_m,g_{m+\Delta m})}$. The oscillation frequencies for σ_{ge} are simply opposite in sign with respect to σ_{eg}, that is, $\zeta_k^{(ij)}=-\zeta_k^{(ji)}$.

In the case of transitions between excited and excited states, or ground and ground states, the matrix T is defined in a slightly different manner; its row elements are composed of $N-1$ integers (i.e., $k_1,k_2,\ldots,k_{N-1}$) satisfying $\Sigma_{j=1}^{N-1}(-1)^j k_j=\Delta m$. To calculate the oscillation frequencies of σ_{ee} or σ_{gg}, we have to perform the different calculation of

$$\sum_{j=1}^{N-1}(-1)^j a_{l_j}^{(ij)}, \tag{22}$$

for all the different sets of l_j $(j=1,2,\ldots,N)$ and i. The typical oscillation frequencies are listed in Appendix for $N=5$ and two-dimensional laser configurations, where the arbitrary $F_g\rightarrow F_e=F_g+1$ transition line is assumed.

Note that for an even number of N, the matrix T is changed; for the eg (ee or gg) transitions, T is defined by all the possible values of integers k_j satisfying $\Sigma_{i=1}^{N-1}(-1)^j k_j=\Delta m$ $[\Sigma_{j=1}^{N}(-1)^j k_j=\Delta m]$. Moreover, when there exist other laser frequencies, we only have to add the frequencies to the

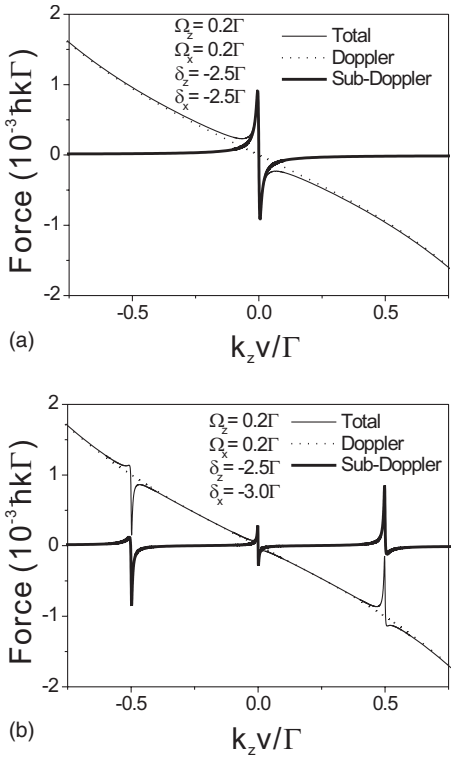

FIG. 3. Calculated forces at $\delta=0.0\Gamma$ (a) and -0.5Γ (b). The total, sub-Doppler, and Doppler forces are represented by thin, thick solid, and dotted curves, respectively.

matrix $a^{(ij)}$. For example, when there exist three laser frequencies with detunings of δ_z, δ_x, and δ_y, the matrix $a^{(ij)}$ is given by

$$a^{(ij)} = \begin{cases} \{k_z v, \delta_1, \delta_2\}, & T_{ij} = -1, \\ \{\delta_1, \delta_2\}, & T_{ij} = 0, \\ \{-k_z v, \delta_1, \delta_2\}, & T_{ij} = +1, \end{cases} \tag{23}$$

where $\delta_{1(2)} = \delta_{x(y)} - \delta_z$.

In summary, the procedure for the calculation of the sub-Doppler forces is summarized as follows. First, we choose the number of interactions (N) and calculate the oscillation frequencies for each matrix element by using the method described in this section. Then, by solving the coupled linear equations [Eqs. (13) and (14)], the matrix elements are calculated. Finally, the forces can be calculated from Eq. (16).

IV. RESULTS

We present the calculated results for the $F_g=1$ to $F_e=2$ transition line in two-dimensional laser configurations. Note that it is straightforward to extend to other transition lines. In the calculation we have employed parameters like those used in typical experiments. The laser detuning and the Rabi frequency for the z axis laser are $\delta_z=-2.5\Gamma$ and $\Omega_z=0.2\Gamma$ (here, Γ is the decay rate of the excited state), respectively.

Figures 3(a) and 3(b) show the calculated forces $F(v)$, where the detuning differences are $\delta=0.0\Gamma$ and $\delta=-0.5\Gamma$, respectively, the Rabi frequency for the transverse laser is $\Omega_x=\Omega_z$, and $B=0$. Here the force is calculated at $x=0$, which implies that the polarization of the transverse laser beams excites only the π transitions. In Fig. 3, the thin, thick solid, and dotted curves represent the total, sub-Doppler, and Doppler forces, respectively. When we calculate the Doppler cooling force, all the ground-state coherences are set to zero. As can be seen in Fig. 3, when the detuning difference is zero [Fig. 3(a)], there exists a sub-Doppler force at $v=0$. However, as the detuning difference becomes nonzero [Fig. 3(b)], the sub-Doppler force at $v=0$ diminishes and new additional sub-Doppler forces available at $v=\pm\delta/k_z$ are created. The qualitative explanation for these resonances will follow below.

As is well known from the study of Ref. [8], in the $\sigma^+ - \sigma^-$ laser configurations, the main origin of the sub-Doppler force is the scattering force, which originates from the population differences in the ground-state sublevels. So we have plotted the populations of the ground-state sublevels in Fig. 4 for $\delta=0$ [Fig. 4(a)] and $\delta=-0.5\Gamma$ [Fig. 4(b)]. In Fig. 4(b), we have only considered the nonoscillating terms among the various oscillating components. The three figures in Fig. 4(c) represent detailed plots of Fig. 4(b) at $v\approx\delta/k_z$, 0, and $-\delta/k_z$ from left to right, respectively. When $\delta=0$ [Fig. 4(a)], the resonance at $v=0$ exhibits abrupt population differences between the sublevels $|g_1\rangle$ and $|g_{-1}\rangle$, which in turn produce a novel scattering force, i.e., the sub-Doppler force. When $\delta=-0.5\Gamma$ (and also at the $v=0$ resonance that is suppressed now), we can observe abrupt changes of the populations at $v=\pm\delta/k_z$, which result in steep sub-Doppler forces at those velocities.

Figure 5 shows the calculated ground-state coherences. If we consider five photon interactions and assume only the π transition is excited from the transverse laser beams, the oscillation frequencies are $-2k_zv$ and $-2k_zv\pm2\delta$ for $\sigma(g_{-1},g_1)$, and $-k_zv\pm\delta$ for $\sigma(g_{-1},g_0)$ and $\sigma(g_0,g_1)$. The real and imaginary parts of the matrix element $\sigma(g_{-1},g_1)$ oscillating at $-2k_zv$, which is the major component, are presented in Fig. 5(a) [Fig. 5(b)] as thick and thin curves for $\delta=0$ ($\delta=-0.5\Gamma$), respectively. The main difference is the decrease of the widths of the coherences in Fig. 5(b), which results in the weak sub-Doppler force at $v=0$ for $\delta\neq0$. The coherences $\sigma(g_{-1},g_0)$ and $\sigma(g_0,g_1)$ have two major components oscillating at $-k_zv-\delta$ and $-k_zv+\delta$. Since the coherence at $-k_zv\mp\delta$ has a resonance near $v=\mp\delta/k_z$, we present the coherences $\sigma(g_{-1},g_0)$ and $\sigma(g_0,g_1)$ oscillating at $-k_zv-\delta$ near $v=-\delta/k_z$ in Figs. 5(c) and 5(d), respectively. The coherences oscillating at $-k_zv-\delta$ can be obtained by symmetry: The real and imaginary parts of $\sigma(g_{-1},g_0)$ [$\sigma(g_0,g_1)$] oscillating at $-k_zv+\delta$ are equal to $\sigma(g_0,g_1)$ [$\sigma(g_{-1},g_0)$] and $-\sigma(g_0,g_1)$ [$-\sigma(g_{-1},g_0)$] oscillating at $-k_zv-\delta$ with $v\rightarrow-v$, respectively. Unlike the coherences at $v=0$, whose real (imaginary) component shows a Gaussian (dispersive) shape, these have somewhat complicated shapes.

In the calculations considered so far, we have assumed that $x=0$, which implies that the laser photons from the transverse directions contribute to only the π transition. However, in real situations, atoms experience complicated polarizations depending on the x value. Here we study this phenomenon in detail, and the results are shown in Fig. 6. The cal-

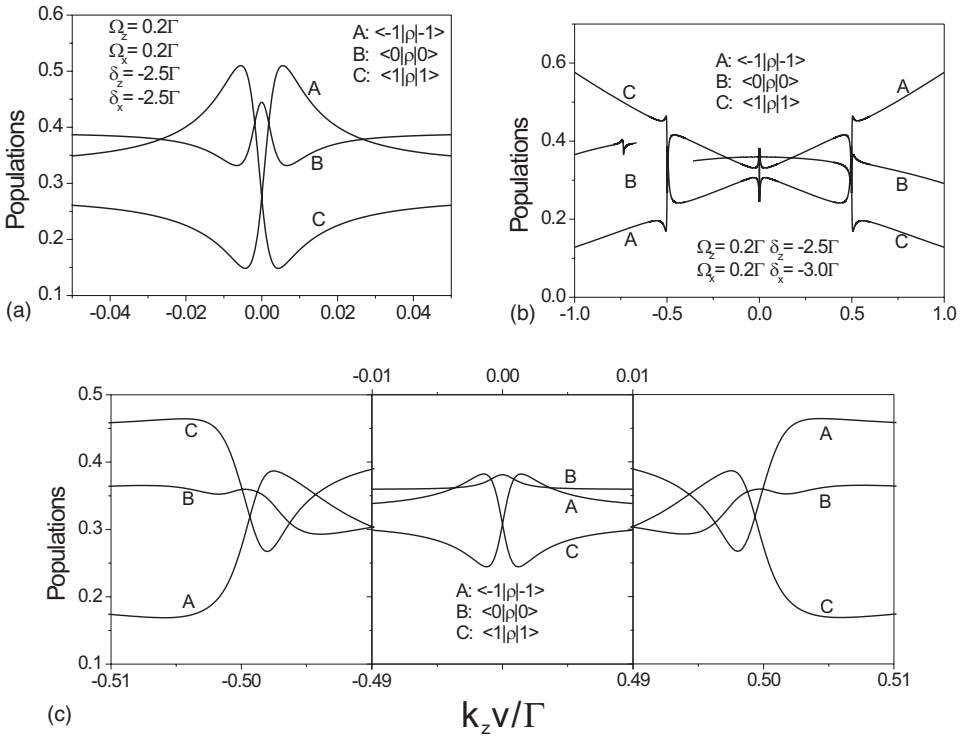

FIG. 4. Populations of the sublevels of the ground state at $\delta=0.0\Gamma$ (a) and -0.5Γ (b). (c) Detailed plots of (b) at $v\sim\delta/k_z$, 0, and $-\delta/k_z$ for the left, central, and right panels, respectively.

culated forces $F(v)$ at $B=0$ and $F(B)$ at $v=0$ are presented in Figs. 6(a) and 6(b), respectively, at the position x from $x=0$ to $\lambda/4$ with a step $\lambda/16$ (λ is the wavelength of the transverse laser beam). The displacement along the x axis is equivalent to the addition of a phase for the reflected beam of the transverse laser beams. For example, when $x=0$, the polarization of the transverse beam is π, while when $x=\lambda/4$, it is equally composed of σ^+ and σ^-. Between these two positions, the polarization is a combination of σ^+, σ^-, and π. In Fig. 6(a), as x changes from $x=0$ to $\lambda/4$, we can see that the strength of the sub-Doppler force at $v=0$ almost remains unchanged, whereas those at $v=\pm\delta/k_z$ slightly decrease. In Fig. 6(b), we can see similar trends as in Fig. 6(a); the force at $B=0$ is almost unchanged but the forces at $B=\pm\hbar\delta/\mu_B$ decrease and finally vanish at $x=\lambda/4$. However, unlike the forces in Fig. 6(a), there exist additional forces at $B=\pm\hbar\delta/(2\mu_B)$, which vanish at $x=0$.

Let us now discuss the mechanism causing the discrepancy in the two calculated forces in Fig. 6. We consider the simple transition diagrams in the right panels of Figs. 6(a) and 6(b). In Fig. 6(a), an atom having a velocity v with $B=0$ is considered. In the absence of the transverse laser beams, the magnetic sublevels of the ground state with $\Delta m=\pm2$, connected by the laser frequencies ω_z-k_zv and ω_z+k_zv, result in coherence at $v=0$, which is the origin of the sub-Doppler force at the MOT center. In the presence of the transverse laser beams at $x=0$, the sublevels with $\Delta m=\pm1$ are connected by π transitions in combination with $\sigma^\pm$ transitions, which leads to the sub-Doppler forces at $v=\pm\delta/k_z$. Also, at $x=\lambda/4$, the transverse laser beams contribute to the $\sigma^\pm$ transitions. Therefore the sublevels with $\Delta m=\pm2$ are coherently connected by the laser frequencies $\omega_z\pm k_zv$ and ω_x, which also results in the sub-Doppler force at $v=\pm\delta/k_z$. Since the transverse laser beams contribute to the resonances at $v=\pm\delta/k_z$ regardless of the x value, the sub-Doppler forces are only slightly changed. In the case of Fig. 6(b), when $x=0$, the resonances occur at $B=\pm\hbar\delta/\mu_B$. However, when $x=\lambda/4$, the coherent connection between the sublevels with $\Delta m=2$ results in the resonances at $B=\pm\hbar\delta/(2\mu_B)$. At positions between $x=0$ and $\lambda/4$, we can observe five resonances. As was reported in the previous paper, these resonances occur as five sub-Doppler traps in the asymmetric MOT [12].

When the intensities are high, we can observe higher-order resonances as presented in Fig. 7. Figures 7(a) and 7(b) show the calculated force $F(v)$ at $B=0$ and $F(B)$ at $v=0$, respectively, where $\Omega_z=\Omega_x=1.5\Gamma$, $\delta_z=-2.5\Gamma$, $\delta=-0.5\Gamma$, and $x=\lambda/8$. As shown in Fig. 6, we can observe two-photon resonances at $v=0$ and $v=\pm\delta/k_z$ for Fig. 7(a) and at $B=0$, $B=\pm\hbar\delta/\mu_B$, and $B=\pm\hbar\delta/(2\mu_B)$ for Fig. 7(b). On the other hand, we can observe four-photon resonances at $v=\pm\delta/3$ for Fig. 7(a) and $B=\pm2\hbar\delta/\mu_B$ for Fig. 7(b). The transition schemes corresponding to these resonances are shown in the right panels of Fig. 7. In the case of Fig. 7(a), the energy conservation relation $\pm\hbar[\omega_z\mp k_zv-(\omega_z\pm k_zv)+\omega_x-(\omega_z\pm k_zv)]=0$ leads to resonances at $v=\pm\delta/3k_z$, where the upper (lower) sign represents the upper (lower) figures. And, in Fig. 7(b), the energy conservation $\hbar(\pm\omega_z\mp\omega_x\pm\omega_z\mp\omega_x)=\mu_BB$ results in the resonances at $B=\mp\hbar\delta/\mu_B$ where the upper (lower) sign denotes the lower (upper) figures.

V. CONCLUSIONS

We have developed an efficient method to calculate the atomic sub-Doppler forces in the presence of bichromatic laser fields and applied it to the case of the asymmetric trap-laser detunings in a six-beam MOT. Instead of expansion in

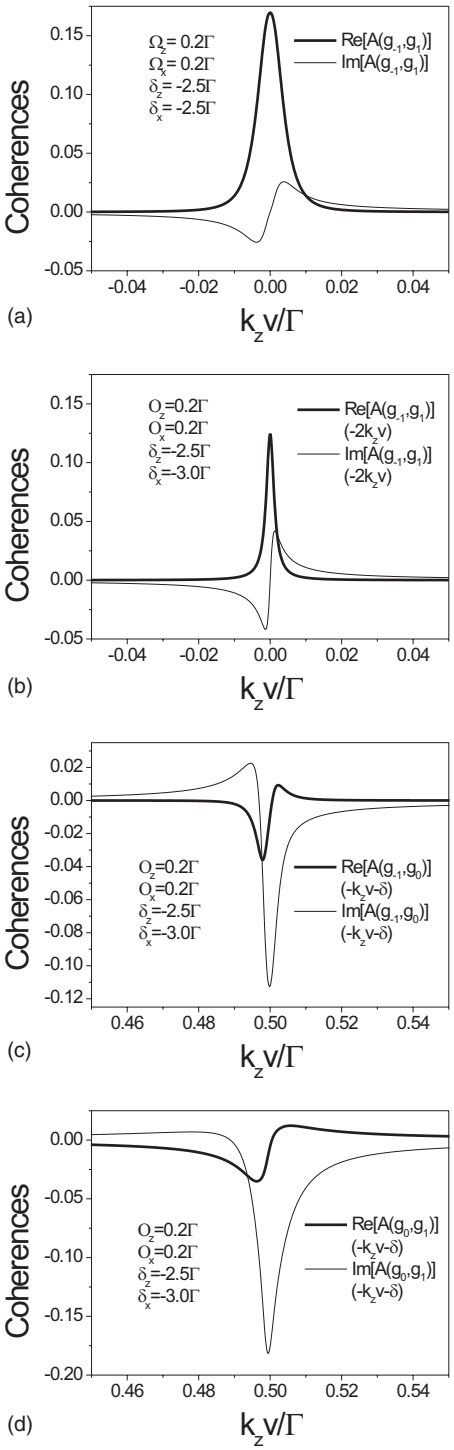

FIG. 5. Real and imaginary parts of the ground-state coherences are presented as thick and thin solid curves, respectively. The ground-state coherence $\sigma(g_{-1},g_1)$ oscillating at $-2k_z v$ at $\delta=0$ (a) and -0.5Γ (b). The ground-state coherence $\sigma(g_{-1},g_0)$ (c) and $\sigma(g_0,g_1)$ (d) oscillating at $-k_z v-\delta$ near $v=-\delta/k_z$.

the Fourier series, we take into account only the nonvanishing terms, which greatly simplifies the calculations. We have been able to explain all the observed effects in the calculations, such as the existence of multiple traps and their physical origins, nonlinear resonances, and three-dimensional array of sub-Doppler traps. Note that in our recent experimental studies we reported multiple sub-Doppler traps in two dimensions [12]. The interesting feature of such multiple sub-Doppler traps is the easy adjustability: We can vary the distances between the traps by merely changing the laser detunings. The calculated forces in the two-dimensional MOT show two peculiar features: one is the suppression or weakness of the sub-Doppler forces at the MOT center and the other is the appearance of additional sub-Doppler forces at $v=\pm\delta/k_z$ when $B=0$. When the stationary atom is considered in a constant magnetic field B, other sub-Doppler forces occur at $B=\pm\hbar\delta/\mu_B$ and $B=\pm\hbar\delta/(2\mu_B)$.

As was observed in the experiment [12], the sub-Doppler forces at the midpoint are very weak compared to the ones at the sides, which is due to the difference of the transition strengths responsible for the sub-Doppler forces. For the three-dimensional asymmetric MOT, one can simply add one more frequency (with a detuning difference δ_1) and consequently sub-Doppler forces at $v=\pm\delta_1/k_z$ are generated. We are currently performing an experiment on the realization of the three-dimensional array of sub-Doppler trap array as expected in this theoretical analysis. We also plan to study the effect of the coherence of each laser wave on the formation of multiple sub-Doppler traps. Moreover, the theoretical calculation method presented in this paper can be extended to a more general case of various laser fields where multichromatic fields exist, and can also be useful for experiments employing the versatile properties of the easily adjustable sub-Doppler trap arrays readily available in an asymmetric MOT.

ACKNOWLEDGMENTS

This work was supported by a Korea Research Foundation Grant funded by the Korean Government (MOEHRD) (Grant No. KRF-2005-041-C00201) and the Korea Ministry of Science and Technology.

APPENDIX

The oscillation frequencies for $N=5$ for the ee and gg transitions are listed as follows. Here $\zeta^{(m,m')}$ represents $\zeta^{(e_{m_e},e_{m_e'})}$ or $\zeta^{(g_{m_g},g_{m_g'})}$ when $m=m_e$ or m_g, respectively. For ee transitions, i.e., $\zeta^{(m_e,m_e+\Delta m)}$, $m_e=-F_e,\ldots,F_e-\Delta m$, and for gg transitions, $\zeta^{(m_g,m_g+\Delta m)}$, $m_g=-F_g,\ldots,F_g-\Delta m$. We denote $u=k_z v$ for simplicity.

$$\zeta^{(m,m)}=\{0,\pm 2\delta,-u\pm\delta,-2u,-2u\pm 2\delta,u\pm\delta,2u,2u\pm\delta\},$$

$$\zeta^{(m,m+1)}=\{0,\pm 2\delta,-u\pm\delta,-2u,-2u\pm 2\delta,u\pm\delta\},$$

$$\zeta^{(m,m+2)}=\{0,\pm 2\delta,-u\pm\delta,-2u,-2u\pm 2\delta,-3u\pm\delta,u\pm\delta\},$$

$$\zeta^{(m,m+3)}=\{0,-u\pm\delta,-2u,-2u\pm 2\delta,-3u\pm\delta\},$$

$$\zeta^{(m,m+4)}=\{0,-u\pm\delta,-2u,-2u\pm 2\delta,-3u\pm\delta,-4u\}. \quad \text{(A1)}$$

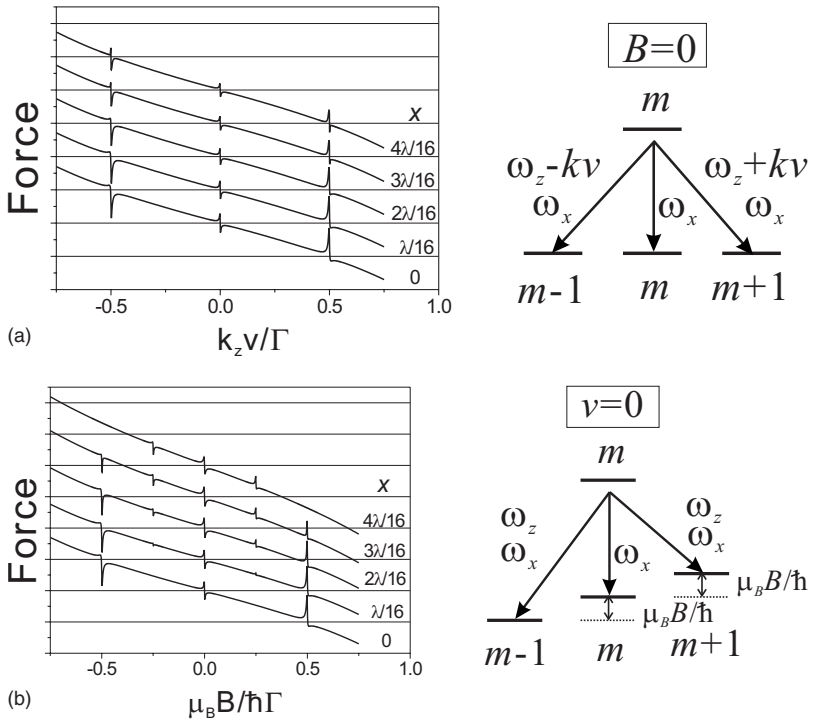

FIG. 6. Calculated forces $F(v)$ at $B=0$ (a) and $F(B)$ at $v=0$ (b) depending on x. The simple diagrams are shown in the right panels.

For the eg transitions, the frequencies are given by the following equations. For $\zeta^{(e_{m-\Delta m},g_m)}$, we have $m=-F_g+\Delta m-1,\ldots,F_g$ with $\Delta m=1,\ldots,N$.

$$\zeta^{(e_m,g_m)}=\{-u,-u\pm 2\delta,-2u\pm\delta,-2u-3\delta,-3u,-3u\pm 2\delta,u,u\pm 2\delta,2u\pm\delta,2u-3\delta,\pm\delta,-3\delta\},\quad \text{for } m=-F_g,\ldots,F_g \tag{A2}$$

$$\zeta^{(e_{m-1},g_m)}=\{-u,-u\pm 2\delta,-2u\pm\delta,-2u-3\delta,-3u,-3u\pm 2\delta,u,u\pm 2\delta,2u\pm\delta,2u-3\delta,\pm\delta,-3\delta\},$$

$$\zeta^{(e_{m-2},g_m)}=\{-u,-u\pm 2\delta,-2u\pm\delta,-2u-3\delta,-3u,-3u\pm 2\delta,u,u-2\delta,\pm\delta,-3\delta\},$$

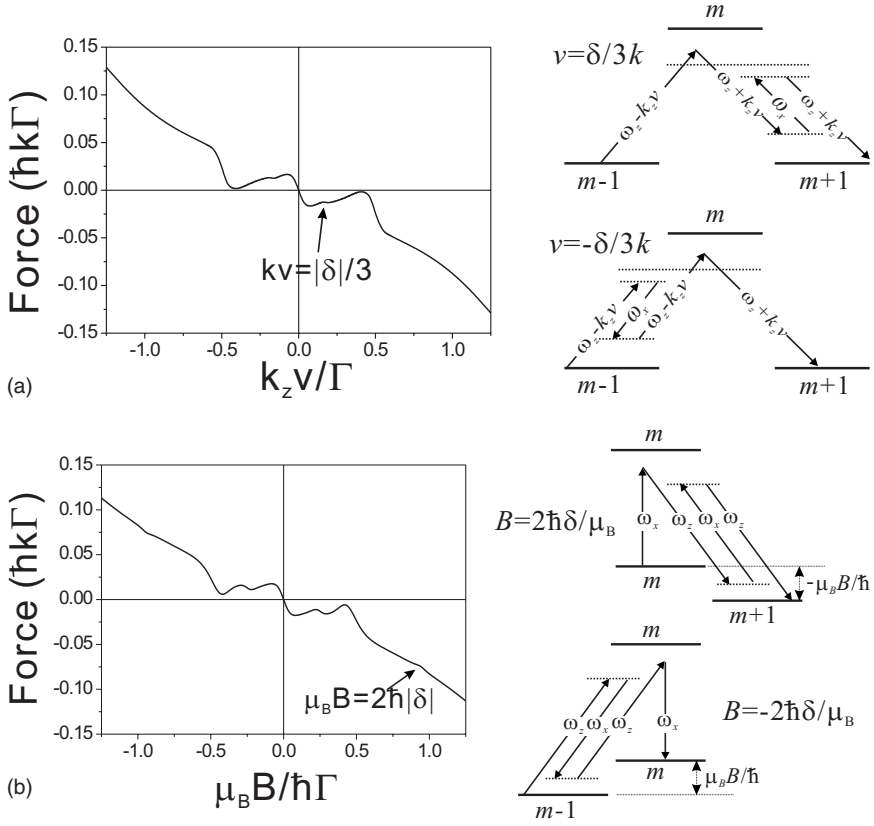

FIG. 7. Calculated forces showing the nonlinear resonances and the transition schemes. (a) The force $F(v)$ at $B=0$ shows the four-photon resonances at $v=\mp\delta/3k$. (b) The force $F(B)$ at $v=0$ shows the four-photon resonances at $B=\pm 2\hbar\delta/\mu_B$. The figures in the right panels show the transition schemes corresponding to each nonlinear resonance.

$$\zeta^{(e_{m-3},g_m)} = \{-u,-u\pm 2\delta,-2u\pm\delta,-2u-3\delta,-3u,-3u\pm 2\delta, -4u\pm\delta,u,u-2\delta,\pm\delta,-3\delta\},$$

$$\zeta^{(e_{m-4},g_m)} = \{-u,-u-2\delta,-2u\pm\delta,-2u-3\delta,-3u,-3u\pm 2\delta, -4u\pm\delta,-\delta\},$$

$$\zeta^{(e_{m-5},g_m)} = \{-u,-u-2\delta,-2u\pm\delta,-2u-3\delta,-3u,-3u\pm 2\delta, -4u\pm\delta,-5u,-\delta\},$$

$$\zeta^{(e_{m+\Delta m},g_m)} = \zeta^{(e_{m-\Delta m},g_m)}(v\rightarrow -v), \quad \text{with } m=-F_g,\ldots,F_g-\Delta m+1, \text{ for } \Delta m=1,\ldots,N. \tag{A3}$$

Also we have the relation

$$\zeta^{(i,j)} = -\zeta^{(j,i)}$$

where $i\neq j$ for all i,j.

[1] T. W. Hänsch and A. L. Schawlow, Opt. Commun. **13**, 68 (1975).

[2] H. J. Metcalf and P. van der Straten, *Laser Cooling and Trapping* (Springer, New York, 1999).

[3] E. L. Raab, M. Prentiss, A. Cable, S. Chu, and D. E. Pritchard, Phys. Rev. Lett. **59**, 2631 (1987).

[4] D. Wilkowski, J. Ringot, D. Hennequin, and J. C. Garreau, Phys. Rev. Lett. **85**, 1839 (2000).

[5] G. Labeyrie, F. Michaud, and R. Kaiser, Phys. Rev. Lett. **96**, 023003 (2006).

[6] K. Kim, M. S. Heo, K. H. Lee, K. Jang, H. R. Noh, D. Kim, and W. Jhe, Phys. Rev. Lett. **96**, 150601 (2006).

[7] P. D. Lett, R. N. Watts, C. I. Westbrook, W. D. Phillips, P. L. Gould, and H. J. Metcalf, Phys. Rev. Lett. **61**, 169 (1988).

[8] J. Dalibard and C. Cohen-Tannoudji, J. Opt. Soc. Am. B **6**, 2023 (1989).

[9] P. J. Ungar, D. S. Weiss, E. Riis, and S. Chu, J. Opt. Soc. Am. B **6**, 2058 (1989).

[10] S. Chang and V. Minogin, Phys. Rep. **365**, 65 (2002).

[11] C. G. Townsend, N. H. Edwards, C. J. Cooper, K. P. Zetie, C. J. Foot, A. M. Steane, P. Szriftgiser, H. Perrin, and J. Dalibard, Phys. Rev. A **52**, 1423 (1995).

[12] M. S. Heo, K. Kim, K. H. Lee, D. Yum, S. Shin, Y. Kim, H. R. Noh, and W. Jhe, Phys. Rev. A **75**, 023409 (2007).

[13] Z. Ficek and H. S. Freedhoff, Phys. Rev. A **48**, 3092 (1993).

[14] P. Zhou and S. Swain, Phys. Rev. A **55**, 772 (1997).

[15] T. H. Yoon, M. S. Chung, and H. W. Lee, Phys. Rev. A **60**, 2547 (1999).

[16] A. Vudayagiri and S. P. Tewari, J. Phys. B **39**, 3919 (2006).

[17] C. Cohen-Tannoudji, J. Dupont-Roc, and G. Grynberg, *Atom-Photon Interactions, Basic Processes and Applications* (Wiley, New York, 1992).